


# Modeling of non-ductile RC structure under near-fault ground motions: A nonlinear finite element analysis

Advances in Structural Engineering  
2022, Vol. 0(0) 1–15  
© The Author(s) 2022  
Article reuse guidelines:  
[sagepub.com/journals-permissions](https://sagepub.com/journals-permissions)  
DOI: 10.1177/13694332221080602  
[journals.sagepub.com/home/ase](https://journals.sagepub.com/home/ase)  


Banu A Hidayat<sup>1,2</sup> , Hsuan-Teh Hu<sup>1,3</sup>, Fu-Pei Hsiao<sup>1,4</sup>, Wen-Cheng Shen<sup>4</sup> ,  
Pu-Wen Weng<sup>4</sup>, Ay Lie Han<sup>2</sup>, Li-Yin Chan<sup>1</sup> and Yanuar Haryanto<sup>1,5</sup>

## Abstract

The old existing reinforced concrete (RC) structures in Taiwan are susceptible to severe damage under earthquakes because of the soft-story mechanism. Moreover, the effects of near-fault ground motions often contain a long period of velocity pulse and permanent ground displacement. This study is based on the tri-axial shaking table test conducted at the National Center for Research on Earthquake Engineering in Taiwan and a series of seismic performance evaluations of a non-ductile RC structure in Taiwan. Finite element analysis (FEA) will be conducted to simulate the linear and nonlinear behavior of the seven-story building. This accommodates the damage plasticity model for concrete and the elastic-perfectly plastic model for reinforcement. Comparison of the results between the experimental test and numerical model showed that the similarity of the vibration period has a great influence on the simulation results. The findings showed that the data of acceleration and displacement behavior corresponded with the experimental results in a satisfactory margin. Also, the damage mode is very similar to the shaking table test results. The study found that using FEA can satisfactorily simulate the seismic performance of mid-rise buildings under a near-fault earthquake.

## Keywords

finite element analysis, near-fault earthquake, non-ductile reinforcement, concrete damage plasticity

## Introduction

Historically, Taiwan has often been hit by strong earthquakes as many active faults have been identified. Hundreds of reinforced concrete (RC) structures have been devastated, resulting in thousands of casualties (Tsai et al., 2000; Zepeda and Hagen, 2016). The collapsed buildings typically exhibit damaged beam-column joints (BCJs), compounded by the non-ductile reinforcing details in columns. Consequently, the existing buildings need to be investigated to enhance their earthquake resistance (Gao et al., 2021; Hidayat et al., 2019; Hsiao et al., 2015; Liou et al., 2002).

Investigation of the seismic performance of RC structures using an experimental program is a tough task from the efficiency and economic aspects. Nevertheless, finite element analysis (FEA) can provide a good approximate solution, compared to laboratory results. Comparing FEA and experimental methods has highlighted the realistic recommendation of validated numerical calculations for the earthquake-resistant structure's design.

The numerical modeling on the RC frames with the infill masonry walls during the construction stages has been conducted. The study shows that the relative errors of the frequencies obtained from the FEA and experimental test were enhanced during the increasing modes (Roudane et al., 2019). The masonry-infilled RC frame has also been

<sup>1</sup>Department of Civil Engineering, College of Engineering, National Cheng Kung University, Tainan, Taiwan

<sup>2</sup>Department of Civil Engineering, Faculty of Engineering, Universitas Diponegoro, Semarang, Indonesia

<sup>3</sup>Department of Civil and Disaster Prevention Engineering, College of Engineering and Science, National United University, Miaoli, Taiwan

<sup>4</sup>National Center for Research on Earthquake Engineering, Taipei, Taiwan

<sup>5</sup>Department of Civil Engineering, Faculty of Engineering, Jenderal Soedirman University, Purbalingga, Indonesia

## Corresponding author:

Fu-Pei Hsiao, National Center for Research on Earthquake Engineering,  
No. 200 Section 3 Xinhai Road, Taipei 106219, Taiwan.  
Email: [fphsiao@ncree.narl.org.tw](mailto:fphsiao@ncree.narl.org.tw)

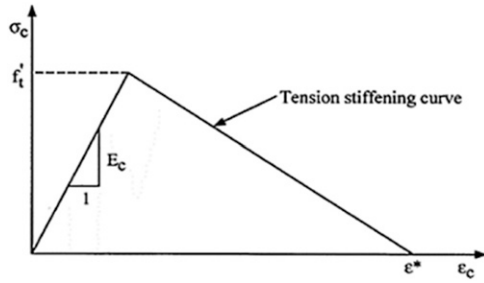


Figure 1. Model of tension stiffening in concrete.

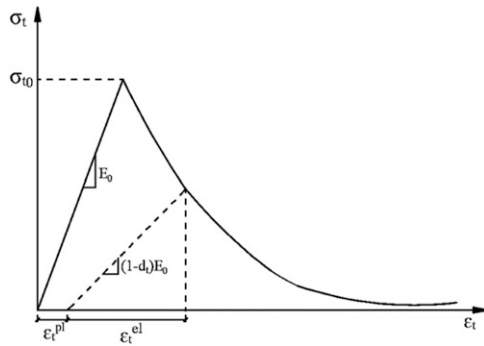


Figure 2. Concrete response under uniaxial tensile loading.

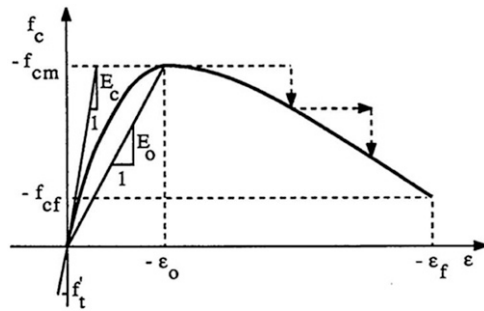


Figure 3. Model of concrete in compression.

investigated through nonlinear cyclic analysis. The comparison between the FE model and the experimental results found that there is a satisfactory agreement of the initial stiffness, cracking pattern, and failure modes of the RC frame (Filippou et al., 2019). There have been a few previous studies contrasting FEA and experiments (Chiou et al., 1999; Kubalski et al., 2016; Mbewee and Zijl, 2018; Mehrabi and Shing, 1997; Redmond et al., 2016; Sattar and Liel, 2016). Yet, the modeling of a massive building previously tested in shaking tables seems comparatively rare.

The important contribution of this study is to examine both linear and nonlinear analyses of the RC building during the near-fault ground motion input, taking into account the effect of the non-ductile reinforcement, along

Table 1. CDP model parameters.

$\psi$	$e$	$f_{bo}/f_{co}$	$K$	viscosity
38	0.1	1.16	0.667	0.00001

Table 2. Details of members of the seven-story building.

Element		Width (cm)	Length (cm)	Height (cm)	Diameter (cm)
Solid elements					
Column A1	CA1	30	30	300	—
Column A2	CA2	30	30	150	—
Column B1	CB1	30	75	300	—
Column B2	CB2	30	75	150	—
Beam 1	B1	30	40	320	—
Beam 2	B2	30	40	275	—
Slab	SL	320	320	10	—
Wall	WA	110	320	15	—
Wire elements					
Rebar-Column		—	—	1200	1.905
Rebar 1-Beam		—	—	720	1.905
Rebar 2-Beam		—	—	715	1.905
Rebar 3-Beam		—	—	370	1.905
Rebar 4-Beam		—	—	365	1.905
Rebar 5-Beam		—	—	150	1.905
Rebar 6-Beam		—	—	127.5	1.905
Stirrup-CA		19.9	19.9	—	0.953
Stirrup-CB		19.9	64.9	—	0.953
Stirrup-Beam		14.9	29.9	—	0.953

with the comparison between shaking table test and computer simulation results of the vibration period similarity.

This research is a continuous project focusing on RC structures that were experimentally tested using a shaking table at the National Center for Research on Earthquake Engineering (NCREE) Taiwan and numerically simulated in FE software (Chan, 2019; Hidayat et al., 2020, 2021; Lin et al., 2020; Pita, 2018; Shen et al., 2018, 2019; Sosa, 2018). The half-scale seven-story RC structure adopted in this study refers to the Golden Dragon building in Tainan, Taiwan, which collapsed in the 2016 Meinong earthquake. This building was designed with non-ductile seismic performance characteristics. A soft-story mechanism occurred in the building, given the larger opening and higher story height on the first floor. Several buildings in Taiwan also had the same condition: vertical irregularity (Chiou et al., 2018).

## Finite element modeling

### Material properties

The same material properties and all the settings of the shaking table test specimen were also built in the FE model.

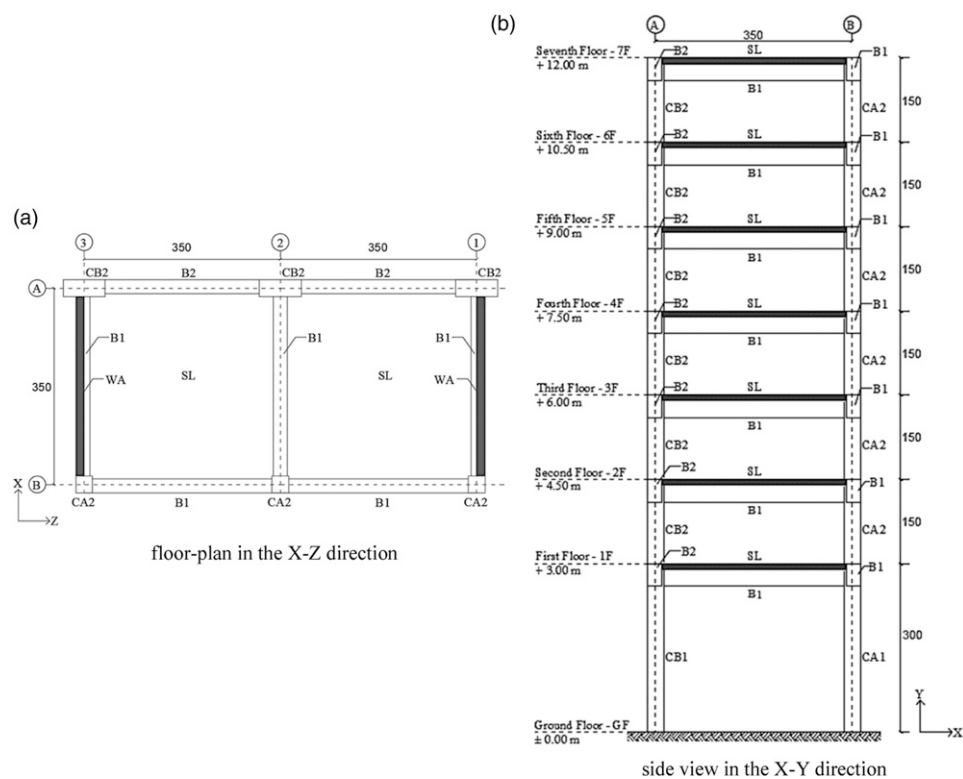


Figure 4. Detailed plan and side view of the building (size in cm).

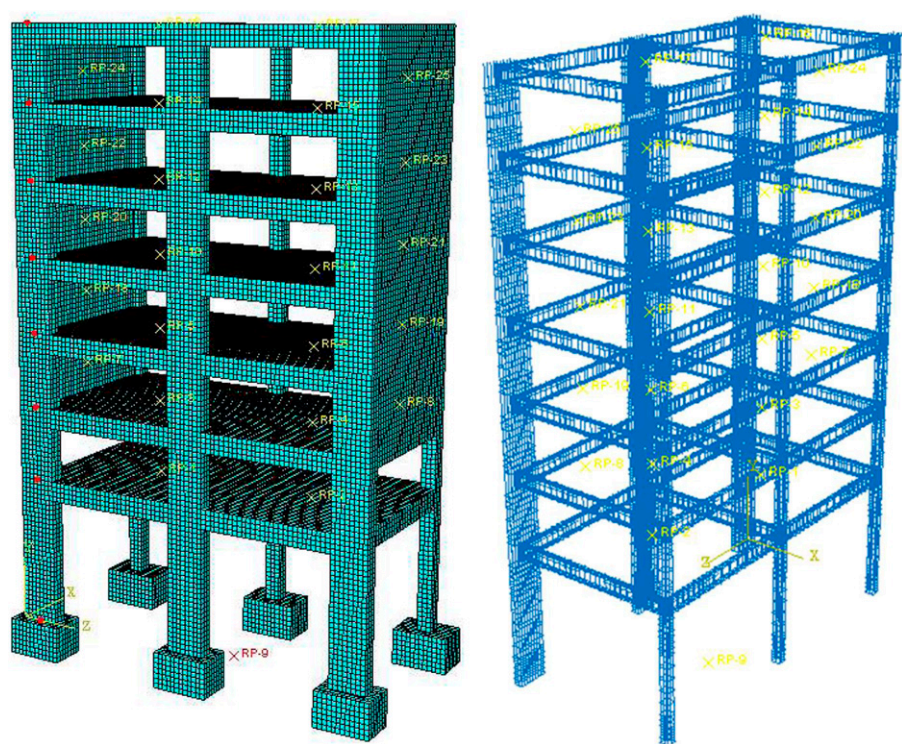


Figure 5. Mesh distribution in the concrete and rebar element.



**Figure 6.** Boundary condition of the building model.

Steel with the yielding stress of 455 MPa and 355 MPa was, respectively, used for 19-mm and 10-mm diameter specimens. The elastic modulus and Poisson's ratio attained are 200 GPa and 0.3, respectively. The elastic-perfectly plastic model for steel was assumed, while the average uniaxial compressive strength of concrete was found to be 20.7 MPa at the 28-day test and the Poisson's ratio was 0.2. The elastic modulus was estimated according to the ACI-318 code (2019) and modified in the Taiwan Design Code (2019).

However, in this study, the elastic modulus of the concrete and reinforcement was reduced by 80% to match the coefficient of Rayleigh damping and the fundamental natural period of the shaking table test results. This assumption was also adopted in the model as the first three-story section of a previous experiment (Lin et al., 2020; Shen et al., 2018) has been reused in this building specimen. Consequently, the material stiffness and elastic modulus need to be adjusted.

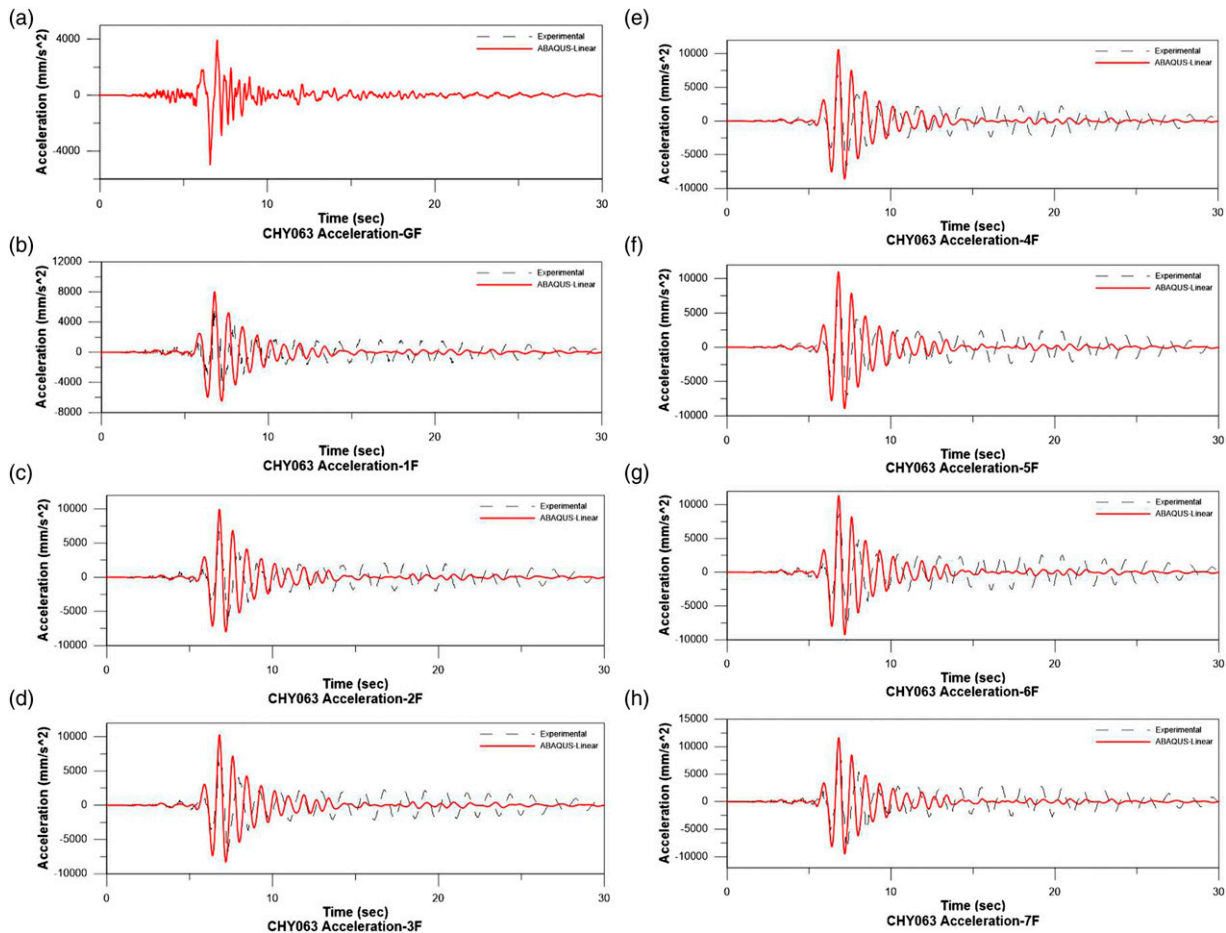


**Figure 7.** Acceleration responses in linear analysis.



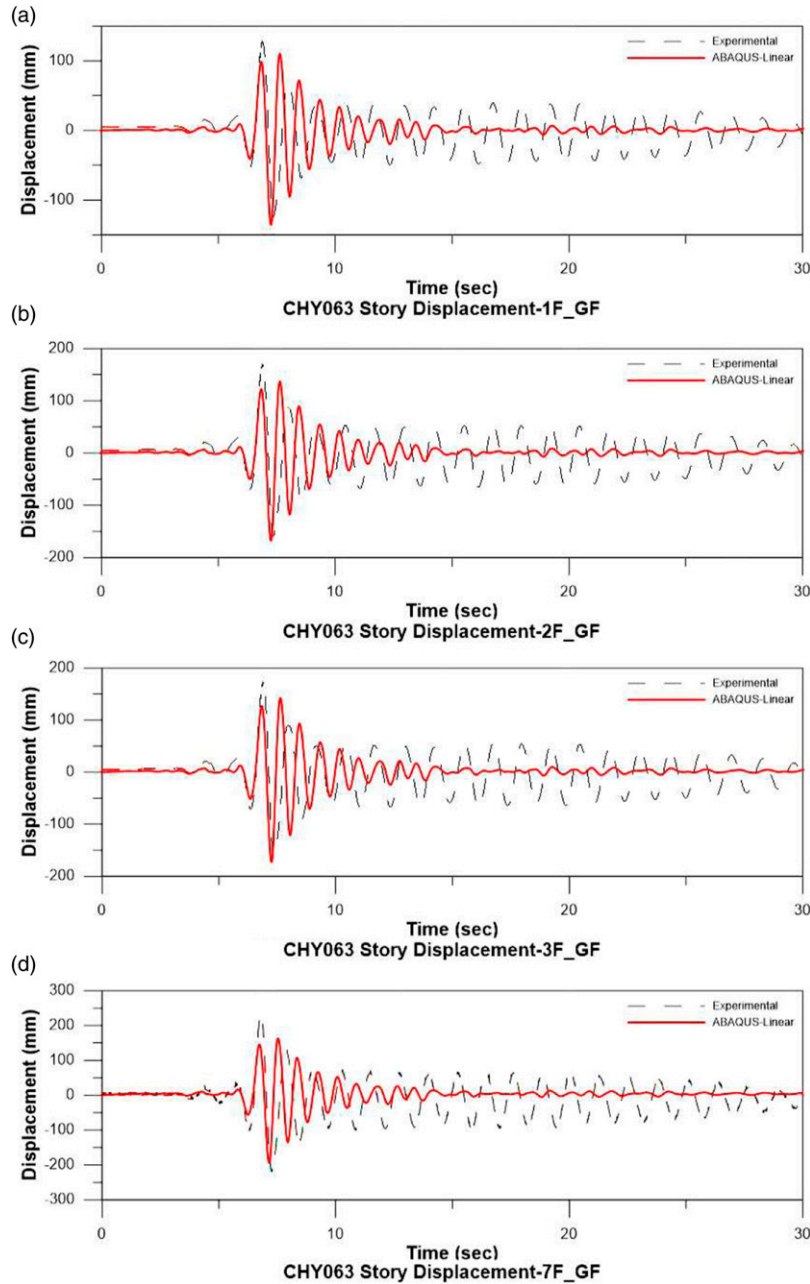


**Figure 8.** Relative displacement responses in linear analysis.

### Constitutive law models

The structural behavior of RC members is rather complex, involving brittle concrete behavior and, conversely, the ductile behavior of steel. This nonlinear response of concrete and steel, respectively, can be represented using plasticity and damage approaches (Alfarah et al., 2017; Indriyantho et al., 2020). Nevertheless, as the presence of the reinforcement brings more ductility, the concrete in RC members can be better described in FEA by using a combined damage and plasticity model.

This aforementioned model leads to the implementation of the concrete damage plasticity (CDP) model in the Abaqus program to show the more detailed seismic behavior of RC buildings. It was taken to accurately represent the inelastic behavior by combining the compressive plasticity and isotropic tensile with scalar damaged elasticity and continuum damage mechanics theory (Haryanto et al., 2021a; Lubliner et al., 1989). In addition, to define the nonlinearity of the concrete, three basic components are needed: plasticity, compressive crushing, and tensile cracking behavior.

The concrete's tension stiffening model in Abaqus is shown in Figure 1 (Hidayat et al., 2021; Systemes D, 2020), with the linear elastic behavior up to tensile strength  $f_t$ , which can be calculated as per the ACI code (2019) to be 1.14 MPa, and after the crack occurred, a simple descending line was formed until the minimum strain value of 0.001. This value was taken close to zero to prevent the potential convergence problem.

The response of concrete under uniaxial tension loading can be characterized by Figure 2, where the softening behavior is marked after the failure stress  $\sigma_{t0}$ . Therefore, the elastic modulus and stiffness will be reduced. This degradation rate can be symbolized by the damage factor  $d_t$  and

**Table 3.** Comparison of experimental and FEA results in linear analysis.

Floor level	Max acceleration (mm/s <sup>2</sup> )		Max displacement (mm)	
	Exp	FEA	Exp	FEA
Ground floor	+3950 −5013	+3940 −4985	— —	— —
1st floor	+6449 −5556	+8004 −6494	+130 −124	+110 −136
2nd floor	+6944 −7075	+9940 −8001	+170 −159	+137 −168
3rd floor	+7,268 −6993	+10,268 −8297	+173 −160	+142 −173
4th floor	+7,610 −6811	+10,621 −8610	— —	— —
5th floor	+8,173 −6997	+10,989 −8932	— —	— —
6th floor	+8,639 −7313	+11,357 −9255	— —	— —
7th floor	+9,218 −7737	+11,626 −9491	+236 −219	+163 −194

formulated in equation (1), which varied from 0 to 1 as undamaged to total damage, where  $\varepsilon_t^{pl}$  and  $E_0$  are, respectively, for the tensile plastic strain and undamaged elastic modulus

$$\sigma_t = (1 - d_t)E_0(\varepsilon_t - \varepsilon_t^{pl}) \quad (1)$$

The curve of stress and strain for concrete under compression (Saenz, 1964) can be shown in Figure 3. Thus, the detailed equation used to construct the stress–strain relation can be indicated in equations (2) and (3)

$$R = \frac{\frac{E_c}{f_{cm}/\varepsilon_o} \left( \frac{f_{cm}}{f_{cf}} - 1 \right)}{\left( \frac{\varepsilon_f}{\varepsilon_o} - 1 \right)^2} - \frac{1}{\varepsilon_f/\varepsilon_o} \quad (2)$$

$$f_c = \frac{E_c \varepsilon_c}{1 + \left( R + \frac{E_c}{f_{cm}/\varepsilon_o} - 2 \right) \left( \frac{\varepsilon_c}{\varepsilon_o} \right)^2 - (2R - 1) \left( \frac{\varepsilon_c}{\varepsilon_o} \right)^2 + R \left( \frac{\varepsilon_c}{\varepsilon_o} \right)^3} \quad (3)$$

where  $f_{cm}$  represents the degraded maximum compressive strength;  $\varepsilon_o$  is for the strain corresponding to  $f_{cm}$ ;  $\varepsilon_f$  is the ultimate compressive strain; and  $f_{cf}$  is the stress corresponding to  $\varepsilon_f$ . Also, the compressive stress at each point on the curve and the initial modulus of elasticity are symbolized by  $f'_c$  and  $E_c$ , respectively.

The plasticity parameters needed for the CDP model are the dilation angle in a deviatoric plane ( $\psi$ ), plastic potential eccentricity ( $e$ ), the ratio of initial biaxial to uniaxial compressive strength ( $f_{b0}/f_{c0}$ ), the ratio of deviatoric stress magnitudes in uniaxial tension and compression ( $K$ ), and viscosity. In this work,  $e$ ,  $f_{b0}/f_{c0}$ , and  $K$  use the suggested values (Hafezolzghorani et al., 2017; Jankowiak and Lodygowski, 2005) and the  $\psi$  and viscosity values are according to the previous study (Hidayat et al., 2021).

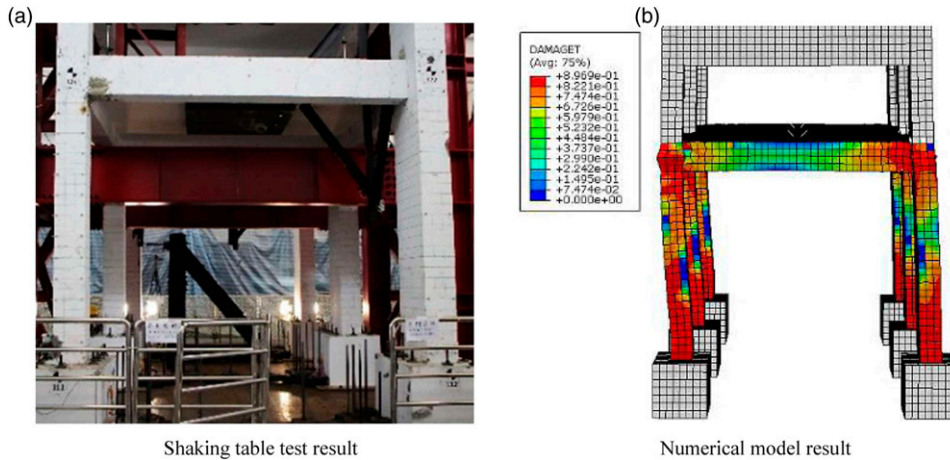


**Figure 9.** Failure mode in inelastic stage (400 Gal).

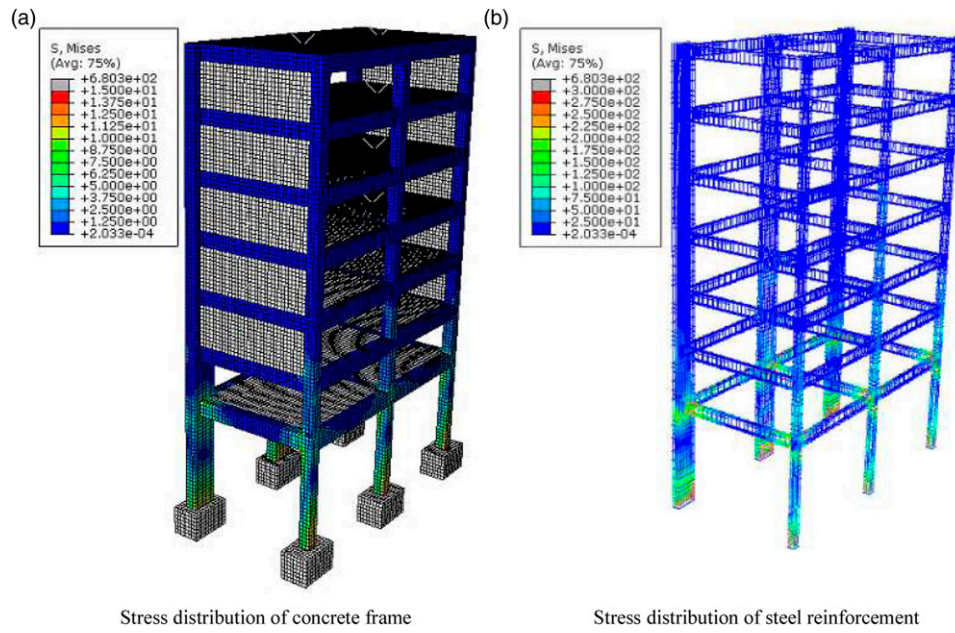


**Figure 10.** Von Mises stress distribution in inelastic stage (400 Gal).

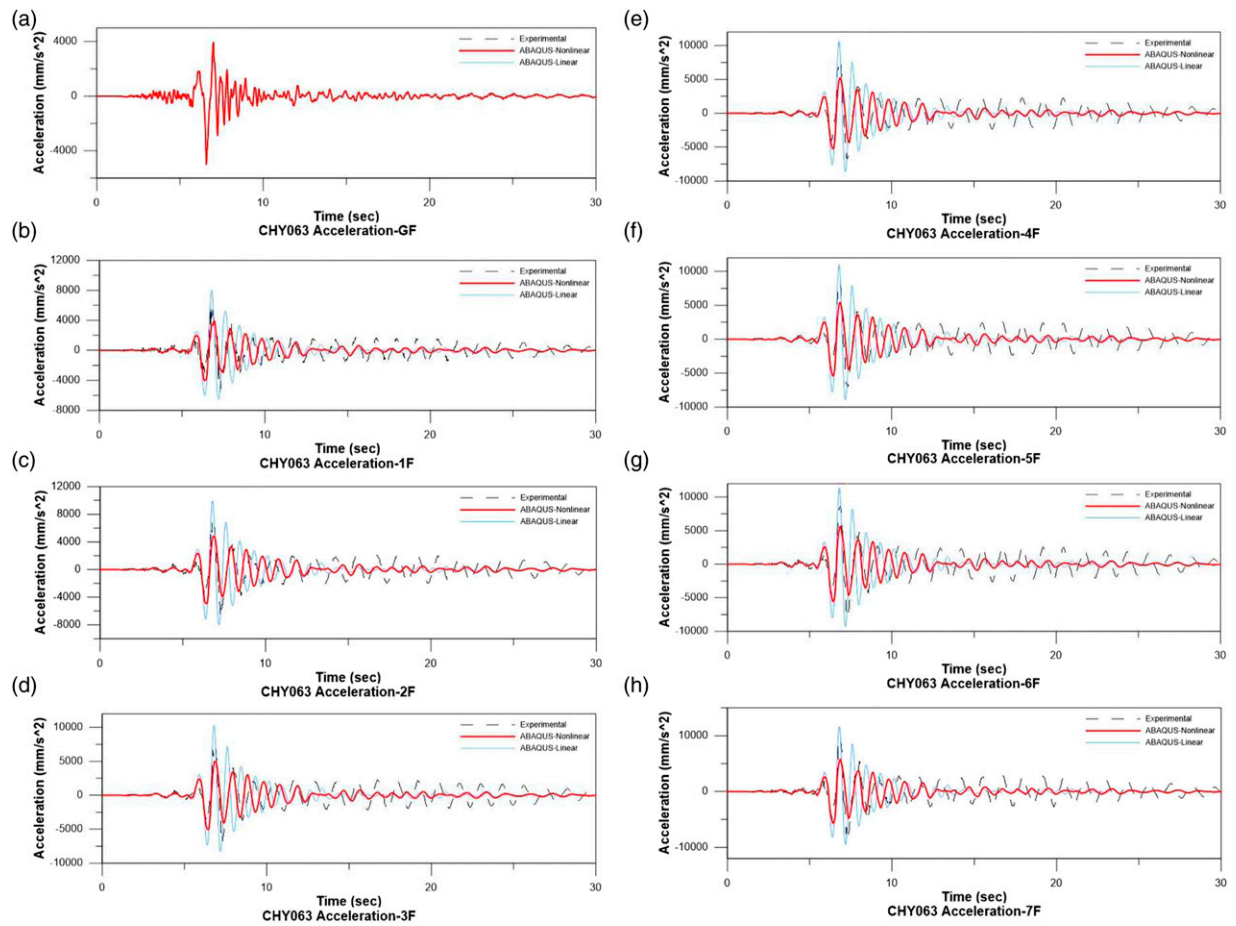


**Figure 11.** Acceleration responses in inelastic stage (400 Gal).

The detailed parameters for the CDP model are given in Table 1, where  $\psi$  represents the dilation angle in a deviatoric plane;  $e$  is for the plastic potential eccentricity;  $f_{b0}/f_{c0}$  is the comparison of the initial biaxial to uniaxial compressive strength;  $K$  is the deviatoric stress ratio; and  $viscosity$  is for the viscoplastic regularization of concrete.

### Seven-story building model

A seven-story building scaled down to 50% was simulated. The sizes of the RC members were exactly the same as

the specimens in the shaking table test (Shen et al., 2018). Two types of column, denoted as CA for a small column with size 30×30 cm and CB as a large column with size 30×75 cm, were connected with beams with the size 30×40 cm and a 10 cm-thick slab. Thus, the reinforcement details and material properties were also the same as the experimental specimen and previous study (Hidayat et al., 2021). Table 2 and Figure 4 show the details of the RC elements and the view of the building, respectively.

However, some modifications were chosen to simplify the model. The perfect bond condition between the concrete

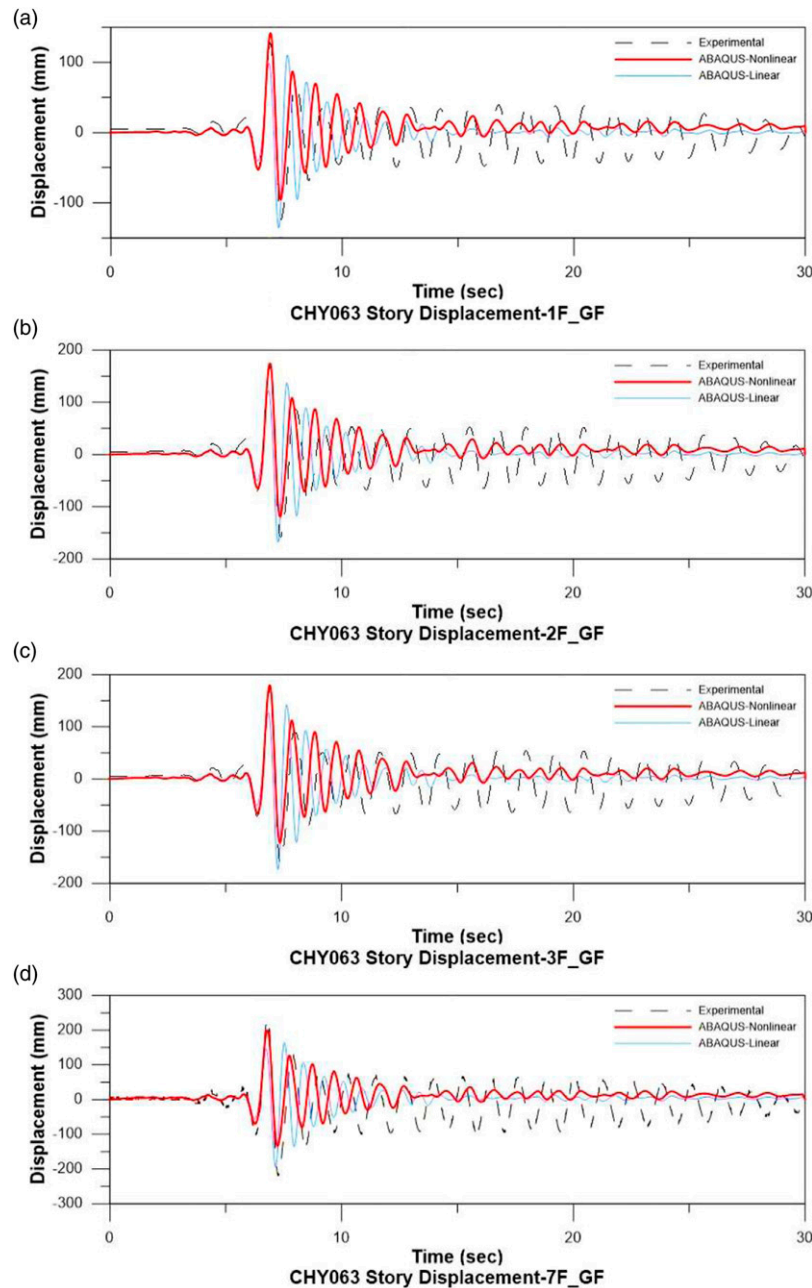


**Figure 12.** Relative displacement responses in inelastic stage (400 Gal).



and the reinforcement was assumed. The cross-ties reinforcements in the columns were omitted and the shear bar arrangement in the BCJs was also neglected. Thus, only the first floor develops plastic behavior and the other floors are still in the elastic condition. The analysis of the foundation, floor, and walls is considered as rigid body motion.

The element type C3D8R, or the reduced integration of eight-node solid elements, was chosen to discretize the concrete material. This type prevents the shear locking effect and simulates the compression hardening and tension stiffening of the concrete very well (Islam, 2020). On the other hand, the longitudinal and transverse reinforcement were simulated with two-node truss elements, T3D2, and embedded throughout the concrete body. Both these element types have three degrees of freedom, translations in the X-, Y-, and Z-direction, for each node. Before implementing the meshing in the seven-story building, the sensitivity analysis was firstly carried out and an appropriate mesh size of 10 cm was used to simulate the concrete and steel bars. The total mesh of the concrete and rebar elements is 55,432 and 40,176, respectively. Figure 5 depicts the meshing distribution of the FE model.

### Loading and boundary condition

This study simulates the seven-story building with similar analysis steps to those of Hidayat et al. (2021). There are two stages of the analysis: the elastic stage to simplify the seismic force behavior and the plastic stage to simulate the structure in an all-around way. The Lanczos method in the Linear Perturbation step was used to solve the eigenvalue equation in the linear analysis. Then the analysis continued by using the Hilber–Hughes–Taylor operator for the non-linear case.

All the RC members are connected by using the Tie Command, which allows members with rapid mesh refinement to be combined as one frame system (Madjour et al., 2017). The steel reinforcements were embedded in the concrete to make them well-wrapped. Thus, after the self-weight condition of the overall model was included, the motion behavior of the underlying base was constrained to the reference point by the Rigid Body Command, as indicated by the constraint at the ground-level floor in Figure 6. The purpose is to directly control the entire constraint area, thus limiting the displacement of the reference point in the Y- and Z-directions, only allowing acceleration works in the X-direction.

The input base acceleration is taken based on the Meinong earthquake, ranging from 400, 600, and 800 Gal seismic force recorded at CHY063 station, as performed in the previous experimental test. This seismic force can be classified as near-fault ground motion with a strong velocity pulse, which may cause permanent ground displacement with a more severe vertical component of ground

**Table 4.** Experimental and FEA results in inelastic stage (400 Gal).

Floor level	Max acceleration (mm/s <sup>2</sup> )		Max displacement (mm)	
	Exp	FEA	Exp	FEA
Ground floor	+3950 −5013	+3940 −4985	— —	— —
1st floor	+6449 −5556	+3900 −4040	+130 −124	+142 −95
2nd floor	+6944 −7075	+4805 −4917	+170 −159	+175 −119
3rd floor	+7268 −6993	+4997 −5071	+173 −160	+180 −122
4th floor	+7610 −6811	+5200 −5235	— —	— —
5th floor	+8173 −6997	+5410 −5403	— —	— —
6th floor	+8639 −7313	+5620 −5577	— —	— —
7th floor	+9218 −7737	+5775 −5704	+236 −219	+200 −134

motion (Alavi and Krawinkler, 2004; Kaveh et al., 2020; Kumar et al., 2015; Mortezaei, 2014; Shuang and Xie, 2007). The pulses are produced by the effects of fling-step and directivity step. These near-fault ground motions have unique properties that are directly related to the mechanism of the earthquake source, the direction of the rupture relative to the site, and the slip direction of the rupturing fault (Alavi and Krawinkler, 2004; Bray and Rodriguez-Marek, 2004; Gerami and Sivandi-Pour, 2013; Mavroeidis, 2004). However, to simplify the analysis time, a total of 110 s of the earthquake is reduced to 30 s. Also, the specimen was scaled down to 50% of the real building.

## Results and discussion

### Seven-story building specimen

**Linear analysis.** In this analysis stage, all the RC members are assumed to be elastic and simulated with a 5% damping ratio. The Dynamic Implicit Method was used to perform the quasi-static load, with the initial size of 0.02 and a total of 1000 increments. The 400 Gal seismic force was taken as the input ground motion. Furthermore, the responses of FEA were recorded in the form of the absolute acceleration and the relative displacement for each floor compared to the ground floor. These parameters could represent the dynamic response of the building.

The measurement points of the building responses are shown in red dots in Figure 5. Moreover, Figures 7 and 8, respectively, illustrate the graphs of the acceleration and

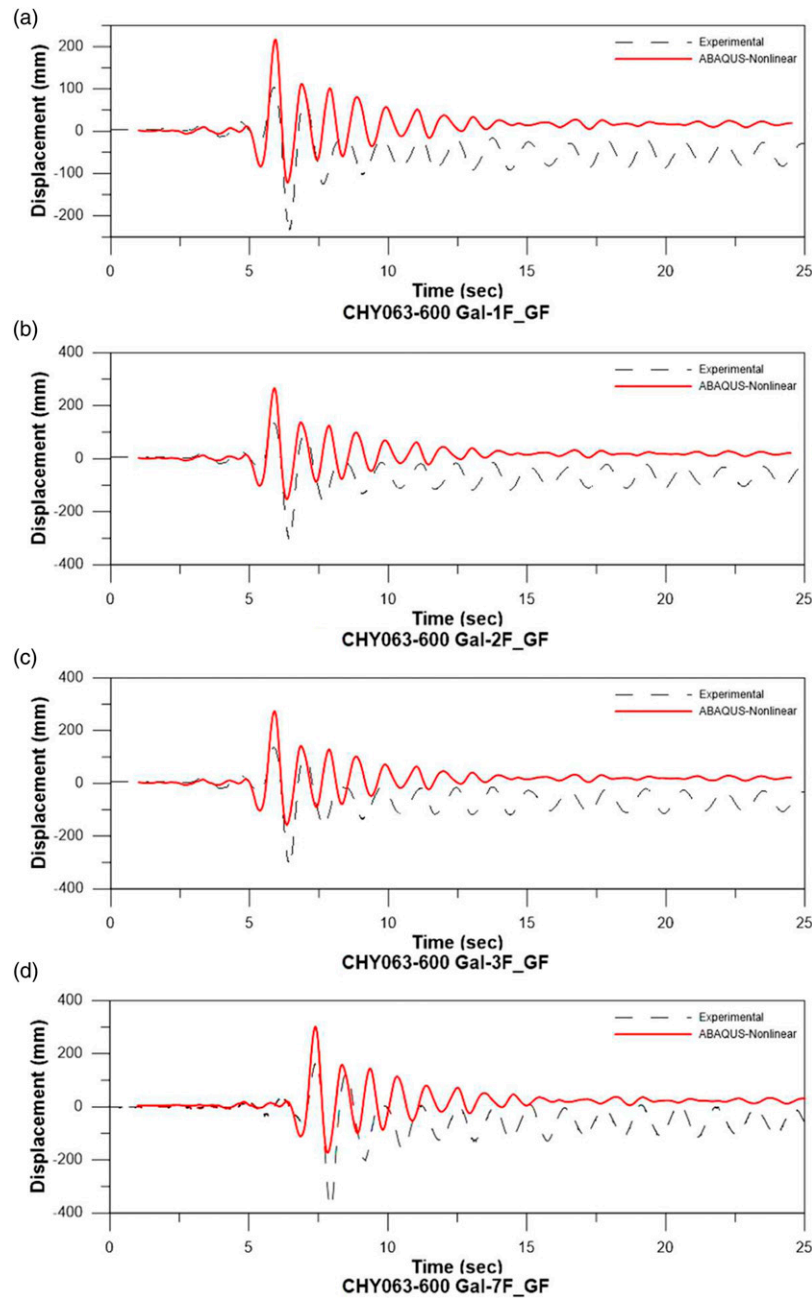


**Figure 13.** Relative displacement responses in inelastic stage (600 Gal).

displacement response of each floor compared with the shaking table test result. It can be seen that the difference between the numerical and experimental results is large in the latter period, as the model is analyzed with elastic materials. However, the harmonic wave motions of the FEA are very similar to the experimental ones as the fundamental period of the model was made to closely match the building specimen.

The maximum acceleration and displacement values during excitation are displayed in Table 3. The acceleration

recorded for each floor increased and, consequently, the displacement response continues to increase. This is in accordance with the research done by Ding et al. (2020). The behavior of the 4<sup>th</sup> to 6<sup>th</sup> floor is still in a linear condition, so the deformation can be assumed to be zero. Also, the presence of the RC wall in the mid-part of the specimen has affected the behavior of the building. In this study, a statistical performance measurement to compare the experimental observation and the numerical prediction was implemented. The normalized mean square error

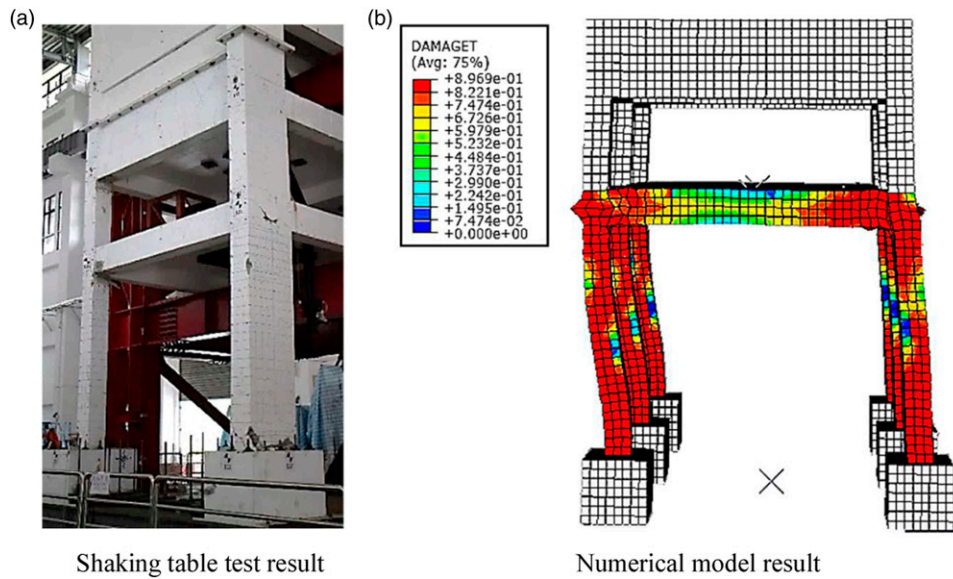


**Figure 14.** Failure mode in inelastic stage (600 Gal).

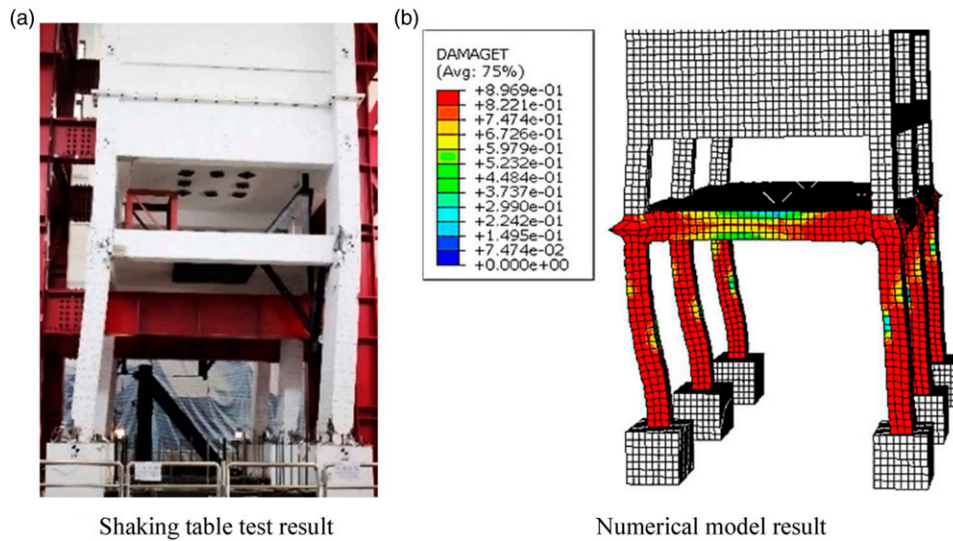


**Figure 15.** Failure mode in collapse stage (800 Gal).

(NMSE) was adopted to evaluate the model efficiencies by measuring the mean relative scatter and reflecting the systematic and unsystematic errors (Asadollahfardi et al., 2019; Haryanto et al., 2021b, 2021c, 2021d; Patryla and Galeriu, 2011; Sirithian and Thepanondh, 2016). The NMSE calculated from the maximum value for the acceleration and displacement response is, respectively, 0.066 and 0.041. These values indicate that the error was still tolerable in the linear stage.

**Nonlinear analysis: 400 Gal.** After the linear stage was applied, the building starts to gradually damage and this condition causes the structure to change from the linear to nonlinear phase as the lateral stiffness drops gradually (Ding et al., 2020). For the first stage of the nonlinear inelastic analysis, the 400 Gal Meinong earthquake ground motion was applied. The same total number of 1000 and the initial size of 0.002 were also chosen for the increment input in the Dynamic Implicit Method. The failure mode

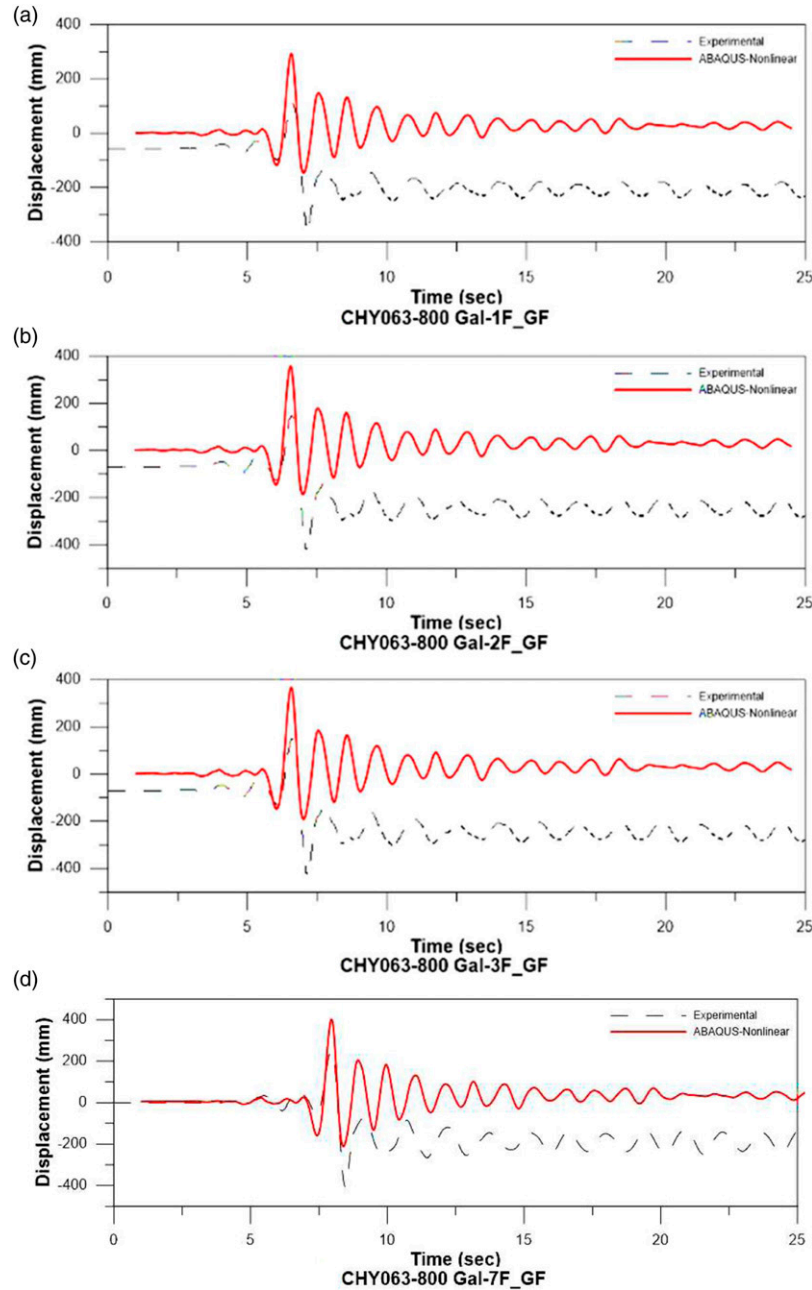


**Figure 16.** Relative displacement responses in collapse stage (800 Gal).

comparison between the FEA and experimental results is shown in Figure 9. The visible results are inclined to the weak column CA, wherein the BCJs and the bottom end of the column are seriously damaged. This condition is following the experimental results. Figure 10 shows the Von Mises stress distributions of the concrete and steel bars. The stress concentration was mainly found in the first-floor columns and BCJs, as the soft-story mechanism occurred.

Further, the acceleration and displacement response of the FEA results compared to the shaking table tests are presented in Figures 11 and 12, respectively. The linear and nonlinear analysis, and experimental responses are, respectively, indicated with blue solid, red solid, and black dashed lines. The maximum response values, taken from the highest data in Figures 11 and 12, are stated in Table 4.

In the shaking table test data, the response in the latter stage is similar to the resonance, which is considered to be



the interaction effect caused by the weak underlayer of the building. Moreover, as the plasticity analysis defines the ultimate strength and nonlinear properties of the concrete, the model enters the nonlinear damage, causes the cycle to increase and brings the response closer to the experimental results. When comparing the acceleration response, the peak value of the nonlinear analysis is, however, not as good as the linear analysis. It is presumed that the softer the material property, the less obvious the amplification effect of the floor. In the relative displacement response, as shown in Figure 12 and Table 4, the percentage difference of the responses is related to the input ground acceleration and plastic energy dissipation.

The error analysis using the NMSE method of the maximum acceleration and displacement response, related to Table 4, are found to be 0.128 and 0.061, respectively. Later, it can be concluded that the error found in the comparison of the experiment and FEA is still in good agreement.

**Nonlinear analysis: 600 Gal.** The relative displacement comparison between the experiment and simulation of the first, second, third, and top floors in the inelastic stage is depicted in Figure 13. The key difference of the residual response is in the size and direction. The black dashed line indicates that the shaking table test had the output value offset about  $-50$  mm, while the red solid line for the simulation had an offset by about  $+20$  mm. This is generally due to the poor behavior of the brittle structure. Figure 14 reveals the damage condition of the experimental and computer analysis at the 600 Gal seismic force. It can be seen that the failure mode of the FEA result is damped in the direction of the weak column. This is in line with the shaking table test result as the weak part of the structure would fail first compared to the stronger members.

**Nonlinear analysis: 800 Gal.** The ultimate damage conditions of the shaking table test and FEA under the 800 Gal seismic force are shown in Figure 15. The final direction of the simulation result is opposite to the experimental test direction. But still, the most damaged part is the first-floor columns and BCJ areas.

Figure 16 illustrates the relative displacement of the first, second, third, and seventh stories, evaluating the numerical and experimental plasticity results. In comparison, the residual response difference is more obvious. The black dashed line indicates that the measurement of the NCREE test is offset by about  $-250$  mm. Yet, in the numerical analysis, the offset of the response is about  $+50$  mm, as indicated by the red solid line. This difference is related to the non-ductile behavior, especially in the lower story, and the limitation of this study regarding the acceleration time-history input in the FE model. The building tilt rate is already in danger of collapse, which led to the collapse stage of the building.

## Conclusions

This study aims to develop the FE model of a non-ductile seven-story RC building, which was hit by a near-fault earthquake. The simulation is performed in linear and nonlinear analysis, then compared to the shaking table test data. The CDP model was chosen to represent the nonlinear behavior of the building during an earthquake.

According to the results and analysis in the aforementioned sections, the following conclusions can be drawn:

1. The soft-story mechanism combined with the old seismic design specification will result in poor structural performances of the RC building. These conditions can be shown by the failure of the first-floor columns and the corresponding beam-column joints.
2. For dynamic analysis, the similarity of the period between the FEA model and shaking table test specimen has a great influence on the subsequent simulation results.
3. The errors calculated between the linear FE analysis and experimental test in the form of the maximum value of absolute acceleration and relative displacement are still tolerable, respectively, for 0.066 and 0.041.
4. In the inelastic stage of the nonlinear analysis, the errors increased to 0.128 and 0.061, respectively. However, the curves of the absolute acceleration and relative displacement with the maximum values show a similar response between the FEA and the shaking table test.
5. The displacement response of the building with the 800 Gal ground motion input indicates that the residual response difference is more obvious, comparing  $-250$  mm and  $+50$  mm respectively for the experimental and model analysis. This condition is related to the non-ductile behavior which led to the collapse stage of the building.
6. The failure modes are also found to be similar for each stage, indicated by the stress concentration in the first-floor columns and BCJ areas.
7. The results in this research have to be seen in the light of a limitation that the displacement time-history input needs to be considered in the future study.

## Declaration of conflicting interests

The author(s) declared no potential conflicts of interest with respect to the research, authorship, and/or publication of this article.

## Funding

The author(s) disclosed receipt of the following financial support for the research, authorship, and/or publication of this article: The research work presented in this paper was supported by NCREE Taiwan.

## ORCID iDs

Banu A Hidayat  <https://orcid.org/0000-0002-8405-238X>  
 Wen-Cheng Shen  <https://orcid.org/0000-0002-1429-9635>

## References

- Alavi B and Krawinkler H (2004) Behavior of moment-resisting frame structures subjected to near-fault ground motions. *Earthquake Engineering & Structural Dynamics* 33: 687–706.
- Alfarah B, López-Almansa F and Oller S (2017) New methodology for calculating damage variables evolution in plastic damage model for RC structures. *Engineering Structures* 132: 70–86.
- Asadollahfardi G, Mazinani S, Asadi M, et al. (2019) Mathematical and experimental study of hydrogen sulfide concentrations in the Kahrizak landfill, Tehran, Iran. *Environmental Engineering Research* 24(4): 572–581.
- Bray JD and Rodriguez-Marek A (2004) Characterization of forward-directivity ground motions in the near-fault region. *Soil Dynamics and Earthquake Engineering* 24(11): 815–828.
- Chan L-Y (2019) *Nonlinear Finite Element 3D Analysis of Non-ductile RC Structures Subjected to Near-Fault Ground Motions*. Tainan, Taiwan: National Cheng Kung University.
- Chiou T-C, Weng P-W, Shen W-C, et al. (2018) *Damaged Building Data of the 2016 Meinong Earthquake in Tainan City, NCREE-18-004*. Taipei, Taiwan: National Center for Research on Earthquake Engineering.
- Chiou Y-J, Tzeng J-C and Liou Y-W (1999) Experimental and analytical study of masonry infilled frames. *Journal of Structural Engineering* 125: 1109–1117.
- Ding X, Chen Z and Xu M (2020) Shaking table experiment of a recycled concrete block masonry building structure with a ‘self-contained’ structural system. *Advances in Structural Engineering* 24(3): 422–436.
- Filippou CA, Kyriakides NC and Chrysostomou CZ (2019) Numerical modeling of masonry-infilled RC frame. *The Open Construction & Building Technology Journal* 13: 135–148.
- Gao F, Tang Z, Mei S, et al. (2021) Seismic behavior of exterior beam-column joints with high-performance steel rebar: experimental and numerical investigations. *Advances in Structural Engineering* 24(1): 90–106.
- Gerami M and Sivandi-Pour A (2013) Performance-based seismic rehabilitation of existing steel eccentric braced buildings in near fault ground motions. *The Structural Design of Tall and Special Buildings* 23(12): 881–896.
- Hafezolzhorani M, Hejazi F, Vaghei R, et al. (2017) Simplified damage plasticity model for concrete. *Structural Engineering International* 27(1): 68–78.
- Haryanto Y, Hu H-T, Han AL, et al. (2021a) Nonlinear 3D model of double shear lap tests for the bond of near-surface mounted FRP rods in concrete considering different embedment depth. *Periodica Polytechnica Civil Engineering* 65(3): 17309. DOI: [10.3311/PPci.17309](https://doi.org/10.3311/PPci.17309).
- Haryanto Y, Hu H-T, Han AL, et al. (2021b) Negative moment region flexural strengthening system of RC T-beams with half-embedded NSM FRP rods: a parametric analytical approach. *Journal of the Chinese Institute of Engineers* 44(6): 553–561. DOI: [10.1080/02533839.2021.1936646](https://doi.org/10.1080/02533839.2021.1936646).
- Haryanto Y, Hu H-T, Han AL, et al. (2021c) Numerical parametric study on the flexural capacity of reinforced concrete beams strengthened with non-metallic materials. *Journal of Engineering Science and Technology* 16(4): 3295–3311.
- Haryanto Y, Hu H-T, Lie HA, et al. (2021d) Numerical investigation on RC T-beams strengthened in the negative moment region using NSM FRP rods at various depth of embedment. *Computers and Concrete* 28(4): 347–360.
- Hidayat BA, Hsiao F-P, Hu H-T, et al. (2020) Seismic performance of non-ductile detailing RC frames: an experimental investigation. *Earthquakes and Structures* 19(6): 485–498.
- Hidayat BA, Hu H-T, Hsiao F-P, et al. (2021) Seismic behavior and failure modes of non-ductile three-story reinforced concrete structure: a numerical investigation. *Computers and Concrete* 27(5): 457–472.
- Hidayat BA, Hu H-T, Han AL, et al. (2019) Nonlinear finite element analysis of traditional flexural strengthening using betung bamboo (*Dendrocalamus asper*) on concrete beams. *IOP Conference Series: Materials Science and Engineering* 615(1): 012073.
- Hsiao F-P, Oktavianus Y, Ou Y-C, et al. (2015) A pushover seismic analysis and retrofitting method applied to low-rise RC school buildings. *Advances in Structural Engineering* 18(3): 311–324.
- Indriyantho BR, Zreid I and Kaliske M (2020) A nonlocal softening plasticity based on microplane theory for concrete at finite strains. *Computers & Structures* 241: 106333.
- Institute AC. (2019) ACI 318–19: building code requirements for structural concrete and commentary.
- Interior Mot. (2019) Design specifications for concrete structures.
- Islam ABMS (2020) Computer aided failure prediction of reinforced concrete beam. *Computers and Concrete* 25(1): 67–73.
- Jankowiak T and Lodygowski T (2005) Identification of parameters of concrete damage plasticity constitutive model. *Foundations of Civil and Environmental Engineering* 6: 53–69.
- Kaveh A, Farzam MF and Maroofiazar R (2020) Comparing H2 and H $\infty$  algorithms for optimum design of tuned mass dampers under near-fault and far-fault earthquake motions. *Periodica Polytechnica Civil Engineering* 64(3): 828–844.
- Kubalski T, Marinković M and Butenweg C (2016) Numerical investigation of masonry infilled RC frames. In: 16th International Brick and Block Masonry Conference. Podova, Italy, 26–30 June 2016.
- Kumar P, Kumar A and Pandey AD (2015) Spectral characterization of Himalayan near-fault ground motion. *Periodica Polytechnica Civil Engineering* 60(2): 205–215.

- Lin J-L, Chen W-H, Hsiao F-P, et al. (2020) Simulation and analysis of a vertically irregular building subjected to near-fault ground motions. *Earthquake Spectra* 36(3): 1485–1516.
- Liou GS, Chiu YF and Cheng FP (2002) Roles of non-structural walls in Chi-Chi earthquake. *Journal of the Chinese Institute of Engineers* 25(4): 473–477.
- Lubliner J, Oliver J, Oller S, et al. (1989) A plastic-damage model for concrete. *International Journal of Solids and Structures* 25(3): 299–326.
- Madjour A, Soltani MR and Harkati EH (2017) Numerical investigation into the ultimate strength of steel cellular beams with semi-rigid connections. *Periodica Polytechnica Civil Engineering* 62(2): 517–532.
- Mavroeidis GP (2004) *Modeling and Simulation of Near-Fault Strong Ground Motions for Earthquake Engineering Applications*. New York, NY: State University of New York at Buffalo.
- Mbewea PBK and Zijl GPAGV (2018) A simplified non-linear structural analysis of reinforced concrete frames with masonry infill subjected to seismic loading. *Engineering Structures* 177: 630–640.
- Mehrabi AB and Shing PB (1997) Finite element modeling of masonry-infilled RC frames. *Journal of Structural Engineering* 123: 604–613.
- Mortezaei A (2014) Plastic hinge length of RC columns under the combined effect of near-fault vertical and horizontal ground motions. *Periodica Polytechnica Civil Engineering* 58(3): 243–253.
- Patryla L and Galeriu D (2011) *Statistical Performances Measures – Models Comparison*. Paris, France: Energies and Atomic Energy Commission. Available at: <http://www-ns.iaea.org/downloads/rw/projects/emras/emras-two/first-technical-meeting/sixth-working-group-meeting/working-group-presentations/workgroup-7-presentations/presentation-6th-wg7-statistical-performances.pdf> (accessed 7 November 2021).
- Pita P (2018) *Studies on Behavior of Non-ductile Reinforced Concrete Columns and Beam-Column Joints Subjected to Cyclic Loading*. Tainan, Taiwan: National Cheng Kung University.
- Redmond L, Ezzatfar P, DesRoches R, et al. (2016) Finite element modeling of a reinforced concrete frame with masonry infill and mesh reinforced mortar subjected to earthquake loading. *Earthquake Spectra* 32(1): 393–414.
- Roudane B, Adanur S and Altunişik AC (2019) Numerical modeling of masonry infilled reinforced concrete building during construction stages using Abaqus software. *Buildings* 9: 191.
- Saenz LP (1964) Discussion of ‘equation for the stress-strain curve of concrete’ by Desayi and Krishnan. *Journal of American Concrete Institute* 61: 1229–1235.
- Sattar S and Liel AB (2016) Seismic performance of nonductile reinforced concrete frames with masonry infill walls-I: development of a strut model enhanced by finite element models. *Earthquake Spectra* 32(2): 795–818.
- Shen W-C, Hsiao F-P, Tsai RJ, et al. (2019) Shaking table test of a reduced scale reinforced concrete structure subjected to near-fault ground motion. In: Pacific Conference on Earthquake Engineering. Auckland, New Zealand, 4–6 April 2019
- Shen W-C, Hsiao F-P, Weng P-W, et al. (2018) Seismic tests of a mixed-use residential and commercial building using a novel shaking table. In: 11th US National Conference on Earthquake Engineering. Los Angeles, CA, 25–29 June 2018
- Shuang L and Xie L (2007) Progress and trend on near-field problems in civil engineering. *Acta Seismologica Sinica* 20(1): 105–114.
- Sirithian D and Thepanondh S (2016) Influence of grid resolution in modeling of air pollution from open burning. *Atmosphere* 7(3): 93.
- Sosa LG (2018) *Finite Element 3D Modeling of Reinforced Concrete Structures Subject to Earthquake Loading*. Tainan, Taiwan: National Cheng Kung University.
- Systemes D (2020) *Abaqus 6.11: Theory Manual*. Vélizy-Villacoublay, France: Dassault Systemes.
- Tsai K-C, Hsiao C-P and Bruneau M (2000) Overview of building damages in 921 Chi-Chi earthquake. *Earthquake Engineering and Engineering Seismology* 2(1): 93–108.
- Zepeda D and Hagen G (2016) Lessons learned from the 2016 Taiwan Mei-Nong earthquake. In: Structural Engineers Association of California Convention. Taipei, Taiwan.